

**Modeling the Shape and Evolution of Normal-Fault  
Facets**

**Gregory E. Tucker<sup>1\*</sup>, Frog<sup>2,1,2</sup>, Frog<sup>3</sup>**

<sup>1</sup>Cooperative Institute for Research in Environmental Sciences and Department of Geological Sciences,  
University of Colorado, Boulder, Colorado, USA.

<sup>2</sup>Frog Pond.

<sup>3</sup>Toad Pond.

**Key Points:**

- What, you're too impatient to read the abstract?

---

\*Current address, McMurdo Station, Antarctica

Corresponding author: A. B. Smith, [email@address.edu](mailto:email@address.edu)

10      **Abstract**

11      this is a highly abstract paper

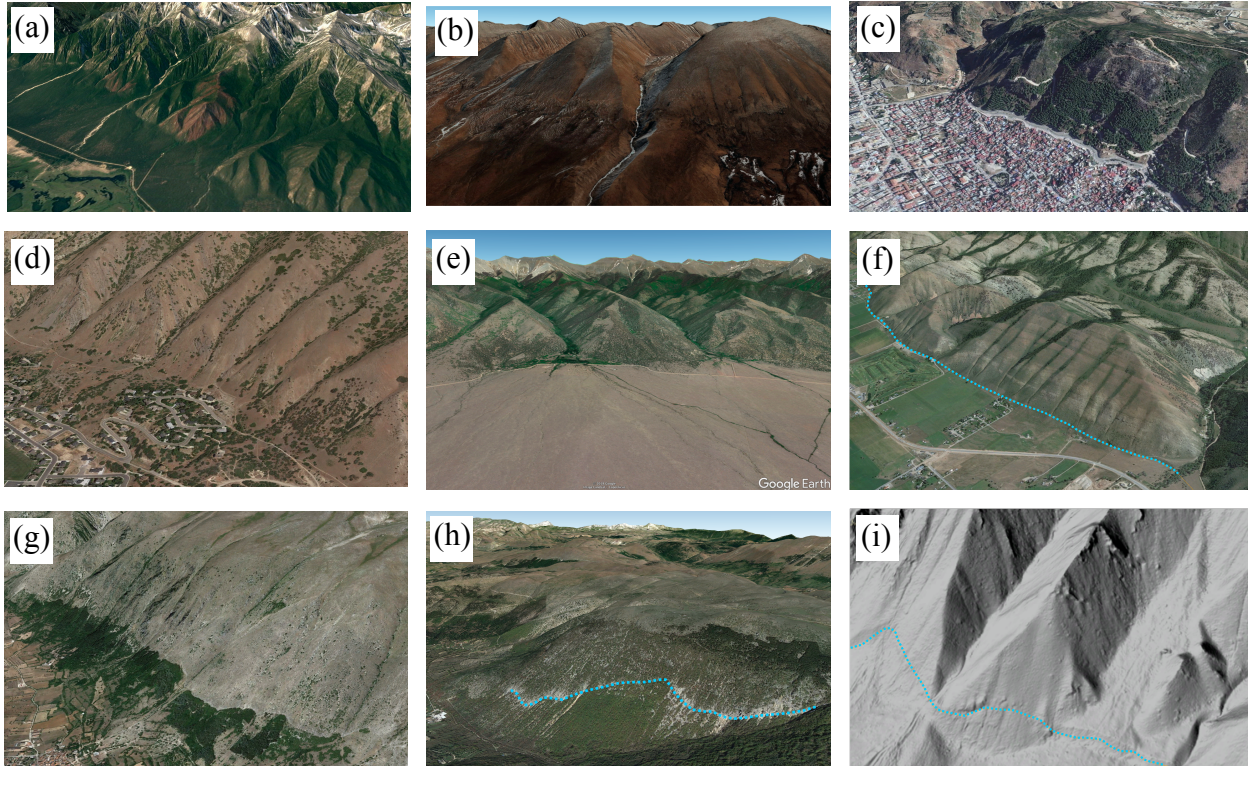
12      **1 Introduction**

13      Mountain ranges in extensional tectonic settings often display fault scarps adorned  
 14      with facets: steep, basin-facing hillslopes that follow the surface trace of the bounding  
 15      fault and mark the transition from footwall to hangingwall (Figure 1). In many cases,  
 16      dissection of a footwall range by transverse streams creates flights of triangular facets:  
 17      facet slopes that are flanked by V-shaped transverse valleys, which present a triangu-  
 18      lar shape when viewed from the adjacent basin (see especially Figures 1a,e,i). In other  
 19      settings, facets may be trapezoidal in profile, or even compose a more or less continu-  
 20      ous surface along a weakly dissected footwall range [e.g., *Wallace*, 1978] (Figure 1g,h).

29      The aim in this paper is to explore the sculpting of facet cross-sectional profiles,  
 30      using a numerical process-based model as an interpretive tool. We examine the extent  
 31      to which the model can account for the diversity in facet morphology, and in particu-  
 32      lar diversity in slope angle, regolith cover, profile shape, and presence or absence of a slope  
 33      break across the range-bounding fault. We also use the model to frame testable predic-  
 34      tions for the relationship between facet morphology, erosion rate, and fault slip rate.

35      **2 Background**

36      Facets have intrigued geologists since at least the late 19th century, when early sur-  
 37      vey expeditions of the American west (and, later, railroad construction) provided access  
 38      to the spectacular terrain of the Basin and Range physiographic province. Among the  
 39      first published remarks and illustrations on facet geomorphology in the western USA were  
 40      those of *Davis* [1903, 1909]. Both he and *Gilbert* [1928] viewed facets as exhumed fault  
 41      planes, with only minor modification by erosion. Later workers, however, noted a dis-  
 42      crepancy between the dip angle of facets and of the fault planes beneath. Where facets  
 43      often dip between 20° and 35° [*Davis*, 1903, 1909; *Pack*, 1926; *Blackwelder*, 1928; *Gilluly*,  
 44      1928; *Fuller*, 1931; *Anderson*, 1977; *Wallace*, 1978; *Menges*, 1990; *Petit et al.*, 2009; *Wilkin-  
 45      son et al.*, 2015], the bedrock fault planes below commonly form angles of 60° to 70° with  
 46      respect to the horizontal [*Schneider*, 1925; *Pack*, 1926; *Blackwelder*, 1928; *Gilluly*, 1928;  
 47      *Fuller*, 1931; *Wallace*, 1978; *Wilkinson et al.*, 2015]. The difference in dip between a nor-



21 **Figure 1.** Examples of normal-fault facets. (a) mountain front in Lake Baikal Rift Zone,  
 22 Russia. (b) Kung Co half graben, Tibet. (c) Hatay Graben, Antakya, Turkey [Boulton and Whit-  
 23 taker, 2009]. (d) Wasatch fault system, Provo section, near Springville, Utah, USA. (e) west  
 24 side of Sangre de Cristo range, San Luis Valley, Colorado, USA. (f) Star Valley fault, Wyoming,  
 25 USA. Note fault trace (light blue dotted line) at base of range front. (g) Magnola fault, central  
 26 Apennines, Italy. Vegetation break marks approximate location of fault trace. (h) Portion of the  
 27 Fucino fault near Gioi di Marsi, Italy. Fault trace shown in light blue dotted line. (i) Wasatch  
 28 fault system, Nephi section, Utah, USA. Fault trace shown in light blue dotted line.

48 mal fault plane and the facets above it implies that facets, despite their often strikingly  
 49 planar form, are erosional features [Pack, 1926; Gilluly, 1928]. Gilluly [1928],  
 50 in his work on the Oquirrh Range (Utah, USA), pointed out an interesting implication  
 51 of this erosional modification: “as the dip of the fault averages more than 60 degrees along  
 52 this part of the range front, a wedge having an apical angle of 30 to 40 degrees has ev-  
 53 idently been removed from each facet.” In other words, because the tip of a facet gets  
 54 exposed to erosion earlier than the base, it undergoes more cumulative erosion. In this

55 sense, the tip of a facet may be considered “geomorphically older” than the base [Gilbert,  
56 1928; Wallace, 1978; Menges, 1990].

57 An unusually well-documented example of the contrast between fault plane and facet  
58 morphology comes from a study of the Campo Felice fault in the Italian central Apen-  
59 nines by Wilkinson *et al.* [2015]. Detailed maps of the Campo Felice fault plane obtained  
60 from terrestrial laser scans of the bedrock fault scarp, together with ground-penetrating  
61 radar images of the fault plane in the subsurface, revealed the fault dip to be  $57\pm4^\circ$ , whereas  
62 the facet surface above the exposed fault plane dips at  $40\pm5^\circ$  and the debris below the  
63 fault trace dips at  $36\pm3^\circ$ . Along the Campo Felice, therefore, Gilully’s “removed wedge”  
64 would have an apical angle of about  $17^\circ$ .

65 Facets show a wide diversity in morphology. Although the dip angles of many facets  
66 range between  $20^\circ$  and  $35^\circ$ , facets have been reported to have dips as low as several de-  
67 grees [e.g., Menges, 1990; Struble *et al.*, in review] or as high as  $\geq 40^\circ$  [e.g., Wilkinson  
68 *et al.*, 2015; Struble *et al.*, in review]. Their apices may vary in height from tens to hun-  
69 dreds of meters. Some facets are more or less continuously mantled in soil, as for exam-  
70 ple those along a portion of the Sangre de Cristo Range in New Mexico, USA studied  
71 by Menges [1990], as well as on some facets along the eastern margin of the American  
72 Basin and Range (Figure 1d,f,i). Others, including facets developed on carbonate rocks  
73 in the Italian central Apennines, are rocky, with a shallow, discontinuous colluvium [Tucker  
74 *et al.*, 2011] (Figure 1g,h). The longitudinal profiles of facets may be planar or convex-  
75 upward. Some faceted mountain fronts display a clear break in slope between the base  
76 of the facets and an adjacent colluvial apron (Figure 1g). For example, hangingwall col-  
77 luvial slopes surveyed by Bubeck *et al.* [2015] in the Apennines showed slope angles of  
78  $20\text{--}25^\circ$ . Along other mountain fronts, the basal colluvium dips at about the same an-  
79 gle as the facet above, with the contact between the two sometimes marked by a fault  
80 scarp (Figure 1h), and sometimes obscure (Figure 1i).

81 The diversity in facet morphology raises the question of whether facets may encode  
82 useful information about tectonic processes, as several studies have suggested. Hamblin  
83 [1976] and Anderson [1977] identified flights of facet-like surface the Wasatch Front (Utah,  
84 USA) separated by bench-like spurs, and interpreted these as reflecting alternating episodes  
85 of rapid slip and tectonic quiescence. Menges [1990] noted that facets along the south-  
86 ern Sangre de Cristo Range tend to be steeper and taller toward the middle of fault seg-

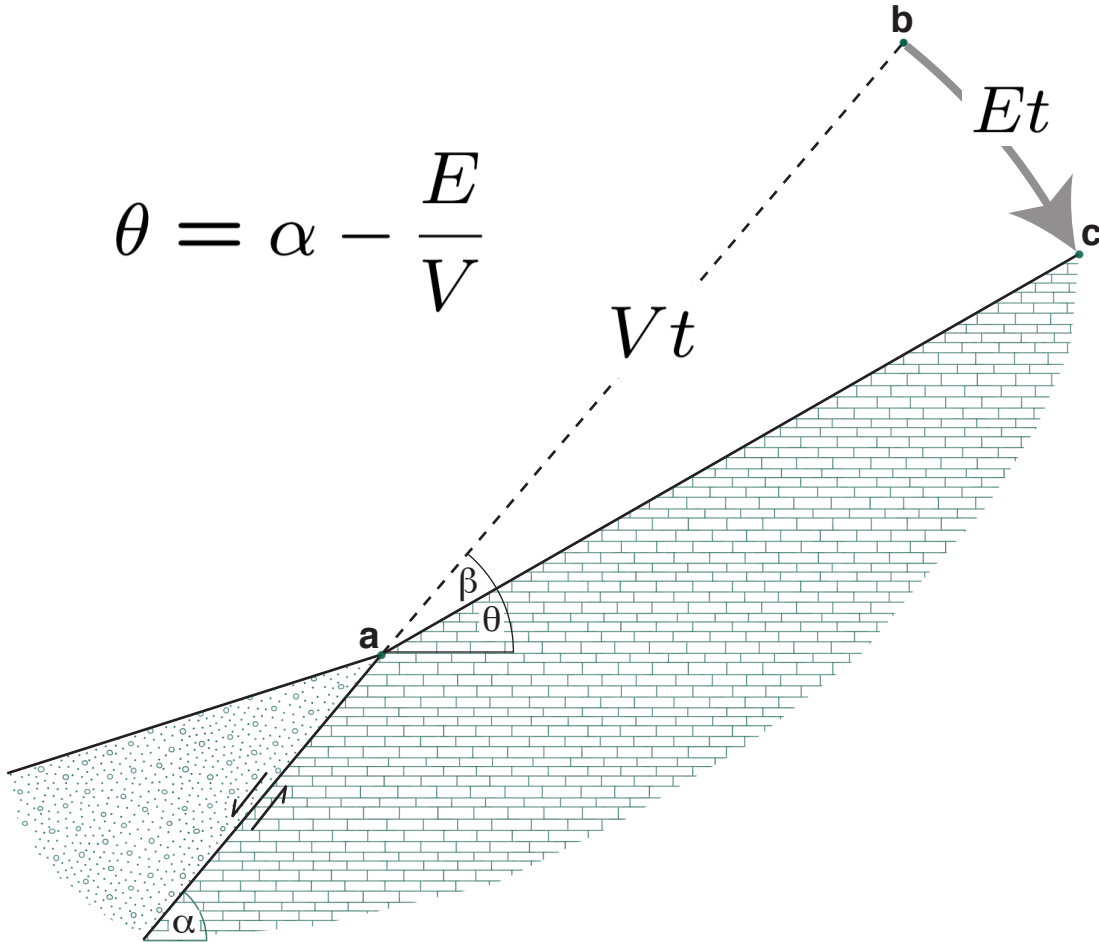
ments, as opposed to zones of overlap between adjacent segments. *DePolo and Anderson* [2000] compiled morphologic data on 45 faults with independent slip-rate estimates in the arid to semi-arid environment of the Great Basin, USA. Faults with a slip rate in excess of a few 10s of microns per year were associated with facets, and among these, *DePolo and Anderson* [2000] demonstrated a correlation between slip rate and facet height. In a study of facets along four segments of the Wasatch fault system, *Zuchiewicz and McCalpin* [2000] noted multiple potential controls on facet geometry, including lithology, but considered slip rate to be the primary control. In laboratory experiments by *Strak et al.* [2011], facet angle increased with slip rate up to a limiting threshold angle. By contrast, *Densmore et al.* [1998] and *Ellis et al.* [1999] suggested on the basis of numerical model experiments that facet erosion might be controlled chiefly by bedrock landsliding, such that facet angle represents a threshold angle for stability that does not correlate with slip rate.

If facets take shape through a collaboration between tectonics and erosion, then it stands to reason that their morphology might also encode useful information about rates of geomorphic processes. *Menges* [1990] noted, for example, that the degree of soil development generally increases upslope on facets along the southern Sangre de Cristo Range. Using a simple geometric model, *Tucker et al.* [2011] noted that the difference in dip angle between a facet and its basal fault—in other words, the apical angle of Gilluly’s wedge of missing rock—could be related quantitatively to the ratio of the rates of fault slip and facet erosion, according to:

$$\beta = \alpha - \theta = E/V, \quad (1)$$

where  $\alpha$  is the fault dip angle,  $\theta$  is the facet dip angle,  $E$  is the slope-normal facet erosion rate, and  $V$  is the fault slip rate. The concept is illustrated in Figure 2. One implication of the geometry illustrated in Figure 2 is that if one knew the fault slip rate and the fault dip, one could estimate the erosion rate (averaged over the age of the facet). Conversely, independent knowledge of the erosion rate would allow estimation of the slip rate.

The geometric view of facets as surfaces that erode as they emerge from below ground leads to the question of what factors determine the erosion rate on a normal-fault facet—and this in turn raises the questions of what are the controlling processes. *Wallace* [1978] hypothesized that fault scarps created by tectonic offset should relax relatively quickly



114 **Figure 2.** Conceptual illustration showing how fault slip rate,  $V$ , fault dip angle,  $\alpha$ , and facet  
 115 erosion rate,  $E$ , combine to set the dip angle of a facet profile. (Modified from *Tucker et al.*  
 116 [2011].)

121 from the initial fault dip to a more stable angle of 30 to 37°, and thereafter lay back much  
 122 more slowly. *Densmore et al.* [1998] and *Ellis et al.* [1999] proposed, on the basis of nu-  
 123 matical model experiments, that many facets form by bedrock landsliding, and that the  
 124 facet surfaces essentially represent failure planes. *Petit et al.* [2009] questioned this in-  
 125 terpretation, in part because of the scarcity of features such as head scarps and debris  
 126 lobes that one would expect to be associated with bedrock landsliding. Our own obser-  
 127 vations of facets in the Italian Apennines and the Wasatch fault system, USA, also lead  
 128 us to support the view of *Petit et al.* [2009] that facets commonly undergo progressive  
 129 weathering and erosion. *Menges* [1990] suggested that facets might be effectively transport-  
 130 limited, yet the fact that some facets have extensive bedrock outcrops suggests that this

is not always the case. Whereas *Menges* [1990] noted some evidence for slope wash, *Gilbert* [1928] argued that “rains accomplish little in the way of erosion... [due to] absorption and retardation by porous talus and in conditions unfavorable to concentration of flow.” Finally, variations in facet morphology and scale with lithology implies that facet materials vary in their susceptibility to weathering and transport [*Menges*, 1990; *Zuchiewicz and McCalpin*, 2000].

Numerical models of extensional mountain range evolution can reproduce classic landforms such as facets, spurs, and wineglass-shaped valleys, but models differ in their representation of the governing processes. *Densmore et al.* [1998] and *Ellis et al.* [1999] introduced a model that included rock weathering, regolith creep, and bedrock landsliding, and explored a part of the parameter space in which facet erosion occurred primarily by landsliding. A model developed by *Petit et al.* [2009] represented hillslope erosion using a diffusion formulation, with a higher transport coefficient applied to slopes steeper than  $40^\circ$ . In their study of facets in the Great Basin, *DePolo and Anderson* [2000] showed that the observed relationship between slip rate and facet angle was consistent with a nonlinear diffusion model. Similarly, analysis of facets along the Wasatch fault system by *Struble et al.* [in review] suggested a nonlinear relationship between erosion rate and facet angle. The planform landscape evolution model studied by *Petit et al.* [2009] showed little correlation between facet slope and fault dip angle, whereas the geometrical analysis of *Tucker et al.* [2011] implies that fault dip should be a primary control. In summary, the community has developed several published models of extensional footwall evolution, but the implications of these models for facet evolution differ depending on the assumed process rules. To make further progress, we need models that can account for the observed diversity in facet morphology, including variations in slope angle, regolith cover, and shape, and that make field-testable predictions about the relationship between morphology, erosion rate, and slip rate.

### 3 Approach and Scope

We view normal-fault facets as unique natural experiments: slopes that are born as steep, seismo-tectonic fault scarps, and undergo progressive weathering and erosion as they are translated upward and away from the fault trace. We use a process-oriented cellular automaton model of facet cross-section evolution as an interpretive tool with which to address the following questions: can the model that combines rock weathering with

disturbance-driven soil creep account for the observed range in facet angle, regolith cover fraction, shape, and colluvial wedge angle? If so, what are the primary controlling factors? Does the model imply a systematic relationship between facet angle and erosion rate, and if so what does that relationship look like? The answer to this last question is especially important, because it sets up a testable prediction: facet angle is easy to measure, and erosion rate can in principle be obtained either through the geometric method summarized in Figure 2 (if fault slip rate is known), or by techniques such as cosmogenic nuclide analysis.

Our focus is on the cross-sectional geometry of facets, rather than their full three-dimensional (3D) form; in other words, our interest is not in explaining why facets are often triangular (which seems to be well understood), but rather in understanding what sets their gradient, shape, and regolith cover. That said, the influence of facet length—the distance between the fault trace and the facet’s upper edge at a particular cross-sectional position—is considered by comparing models with varying domain length, as described below. We do not consider controls on the height of the facet edge, as this clearly depends in part on the spacing between transverse channels, and on the topography of valley side slopes along them.

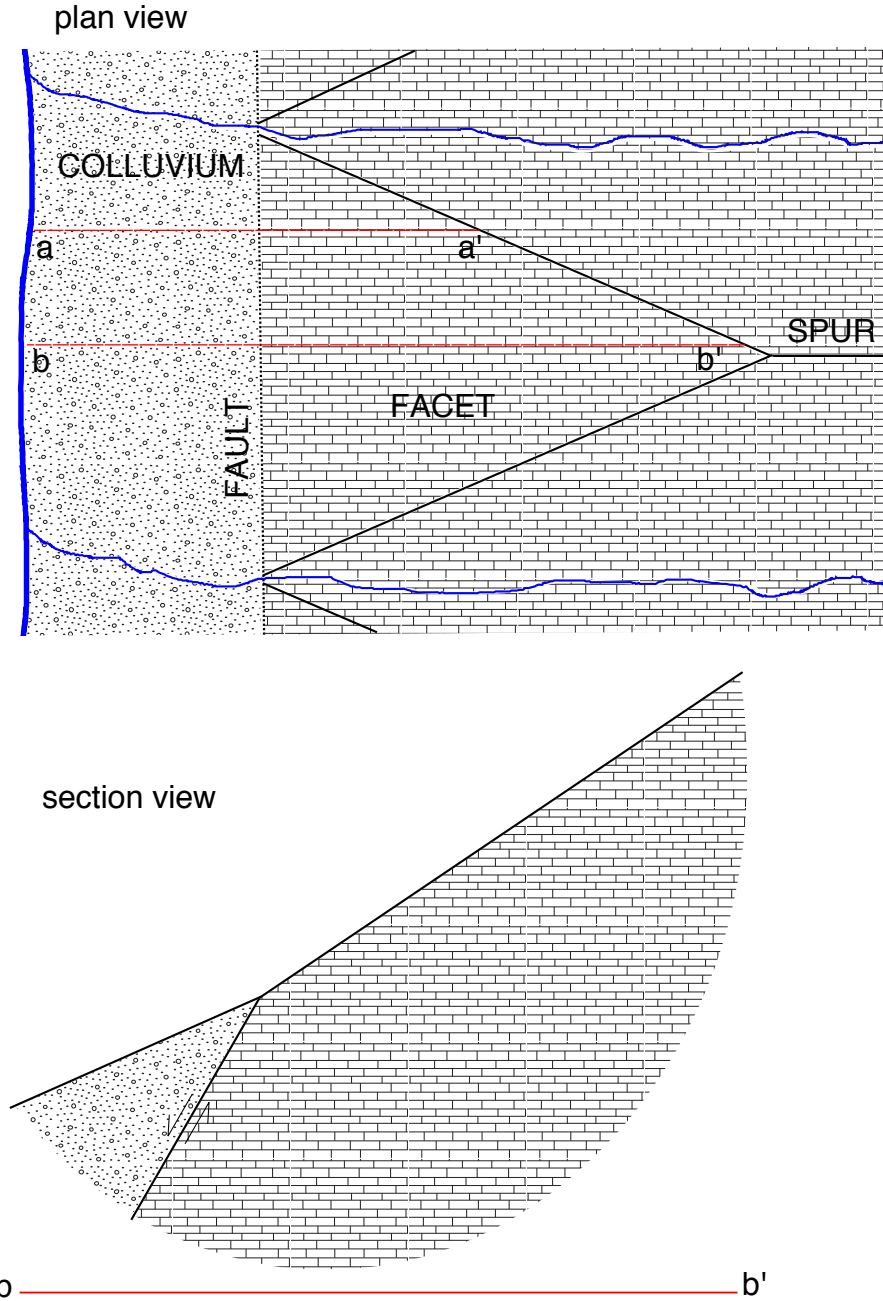
A cellular automaton model might seem like an odd choice for modeling the evolution of an idealized hillslope cross section. After all, most models of hillslope cross-sectional morphology are built on differential equations, which are sometimes viewed as “the keys to geomorphic nirvana” [Bras *et al.*, 2003]. In this case, however, it is the only model we know of that can account for both smooth, soil-mantled slopes, and steep, irregular, rocky ones—and the transition between these forms [Tucker *et al.*, 2018]. Moreover, the cellular framework allows a fully two-dimensional representation (as opposed to the more common profile representation, in which surface elevation is a function of one independent spatial dimension), and it provides a natural way to treat combined vertical and horizontal tectonic offset. Finally, the cellular approach described below (and in greater detail by Tucker *et al.* [2018]) honors the occurrence of a patchy or otherwise incomplete regolith cover, as is observed on some facet surfaces.

Section so-and-so does X, then Y, etc...

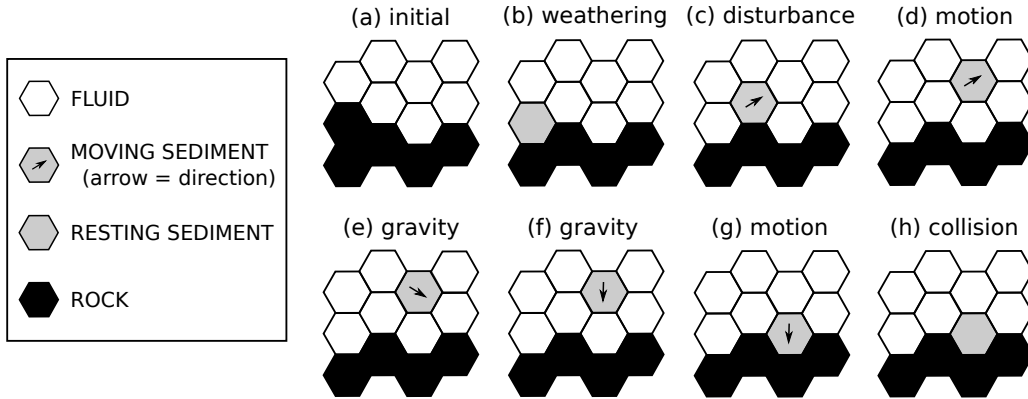
193      **4 Cellular Hillslope Evolution Model**

194      The facet profile evolution model builds on “Grain Hill” cellular automaton frame-  
 195      work [Tucker *et al.*, 2018], with the addition of a 60° dipping normal fault. Advantages  
 196      of the Grain Hill model include the ability to reproduce a range of hillslope forms, from  
 197      soil mantled to rocky; representation of short-range and long-range (“nonlocal”) sedi-  
 198      ment motion, depending on topography; direct treatment of stochastic disturbance; and  
 199      ability to relate model parameters to the more commonly used transport and weather-  
 200      ing rate coefficients. The model domain consists of a lattice of hexagonal cells that rep-  
 201      resents a vertical cross-section through a hypothetical facet and its adjacent colluvial wedge  
 202      (Figure 3). The lower left corner of the model represents a longitudinal stream that re-  
 203      moves any debris delivered to it, and whose elevation is fixed to the hangingwall block,  
 204      which serves as the reference frame for the model. The right side of the model represents  
 205      the upper edge of the facet at that particular cross-section; increasing or decreasing the  
 206      width of the domain equates to moving the cross section toward or away from the facet  
 207      tip (Figure 3).

214      Each hexagonal model cell represents one of three types of material: air, rock, or  
 215      regolith (Figure 4). Regolith cells may be stationary, or may be in a state of motion in  
 216      one of the six lattice directions. Collectively, these materials and motion directions are  
 217      represented by assigning one of nine integer state codes to each cell in the domain. Stochas-  
 218      tic, pairwise transitions represent the processes of rock weathering, regolith disturbance,  
 219      and ensuing regolith motion [Tucker *et al.*, 2016, 2018]. For example, the rock cell in rock-  
 220      air pair has a user-specified probability per unit time of transitioning to a regolith cell,  
 221      representing weathering. Instead of clicking through a series of time steps of fixed du-  
 222      ration, the model iterates over a sequence of these stochastic transitions, in which one  
 223      or both cells in an adjacent pair changes state. The algorithm works by scheduling each  
 224      potential transition event at a randomly generated future time, using an exponential prob-  
 225      ability distribution function of inter-event waiting times. The program then iterates in  
 226      chronological order through these scheduled events. As the domain evolves, new trans-  
 227      sitions are scheduled, and some previously scheduled ones are invalidated. Tucker *et al.*  
 228      [2016] provide further details on the continuous-time stochastic framework and the al-  
 229      gorithms that implement it.



208      **Figure 3.** Schematic illustration of model domain, which represents vertical cross-section  
 209      through an idealized facet and its adjacent colluvial wedge (a–a'). Right side of domain repre-  
 210      sents the upper edge of facet, and left side represents a longitudinal stream in the hangingwall  
 211      that removes any debris delivered to it. Changing the position of the cross section (for example,  
 212      from a–a' to b–b'), and therefore its length, is accomplished by changing the width of the model  
 213      domain.



230      **Figure 4.** Illustration of cell states and pairwise transitions in the Grain Facet model. Each  
 231      cell assigned an integer from 0 to 8 that represents its state (0 is fluid, states 1–6 represent the  
 232      six directions of motion, state 7 is resting sediment, and state 8 is rock). (Figure modified from  
 233      *Tucker et al. [2018]*).

234      *Tucker et al. [2018]* present the rule set for the Grain Hill model. Here, we briefly  
 235      summarize these rules, and describe two additions to the version they present: the im-  
 236      plementation of periodic slip on a  $60^\circ$  dipping normal-fault, and the addition of a rule  
 237      that represents dissolution of bedrock.

238      To represent normal-fault slip, a  $60^\circ$ -dipping fault crosses the grid lattice at a user-  
 239      specified location (Figure 3, bottom). Cells in the footwall block are shifted up and to  
 240      the right on a  $60^\circ$  angle, at a distance of  $\sqrt{3}$  lattice units per time interval  $\tau$ . The slip  
 241      rate is therefore  $V = \sqrt{3}\delta\tau$ , where  $\delta$  [L] is the width of a grid cell.

242      Production of moveable regolith from bedrock is represented by a transition from  
 243      a rock-air pair to a regolith-air pair (Figure 4a,b). The rate constant  $w$  [1/T] represents  
 244      the average transition frequency. Given a cell width of  $\delta$ , the expected bare-bedrock weath-  
 245      ering rate is  $2\delta w$  (the factor of two reflects the fact that for a planar surface, the hex lat-  
 246      tice geometry exposes an average of two faces per cell).

247      In order to explore the case of fully weathering-limited slopes, we introduce a sec-  
 248      ond weathering rule to represent dissolution. When this rule is invoked, rock-air cell pairs  
 249      transition to air-air pairs—representing rock dissolution—with an average rate  $s$  [1/T].  
 250      The expected bare rock dissolution rate [L/T] is therefore  $\delta s$ .

We assume that regolith transport can occur by two means: (1) displacement by a disturbance event and subsequent motion, or (2) spontaneous gravitational failure, when the local angle of repose is exceeded. The model's disturbance rule represents the action of processes like animal burrowing, frost heave, tree throw, and other mechanisms that tend to displace regolith outward from the surface. The disturbance transition rule applies to locations where a resting regolith cell lies adjacent to an air cell. When the transition occurs, regolith and air cell trade places, and the regolith state switches from resting to moving in the direction from which disturbance originated (Figure 4b,c). The disturbance rate parameter,  $d$  [1/T], represents the average disturbance frequency, and functionally equates to the disturbance frequency parameter  $N_a$  in the probabilistic theory of soil creep developed by *Furbish et al.* [2009]. *Tucker et al.* [2018] show that for relatively gentle slopes, the disturbance rate relates directly to the commonly used soil transport efficiency factor (“hillslope diffusivity”),  $D_s$ , according to

$$d = \frac{D_s}{60\delta^2}. \quad (2)$$

For regolith-mantled slopes steeper than about 15°, the effective transport efficiency increases progressively with slope angle, diverging at a 30° effective angle of repose [*Tucker et al.*, 2018, , their Figure 10].

Moving particles follow a set of transition rules that mimic the kinematics of inelastic grain motion in a gravitational field. Although these motion and collision rules are necessarily heuristic, they effectively capture the settling motion of disturbed particles [*Furbish et al.*, 2009]. The motion, gravitational, and inelastic collision rules are illustrated in Figure 4, and described in greater detail by *Tucker et al.* [2016] and *Tucker et al.* [2018]. One rule to note in particular: a regolith cell that lies above and adjacent to an air cell can transition to a moving state, with a high transition rate parameter. Because of the lattice geometry, this rule imposes an effective 30° angle of repose.

Sensitivity experiments indicate that the exact nature of the motion and settling rules is not especially important. What matters more is that there exists a time-scale separation between disturbance (with intervals on the order of years) and settling (time scale on the order of seconds or less). The rule set described above can capture a range of slope forms, including regolith-mantled and convex-upward forms, planar angle-of-repose, and partially mantled “rocky” slopes [*Tucker et al.*, 2018].

This generality makes the model an appropriate one for exploring bedrock fault scarps and facets, which emerge during earthquakes as steep, rock slopes, and can subsequently evolve into partially or fully regolith mantled erosional slopes. In the following section, we present model experiments that address three related questions:

1. What conditions are both necessary and sufficient to produce planar facet profiles with a thin mantle (continuous or discontinuous) of regolith?
2. Can the model account for the observed range in facet slope angle, cross-sectional shape, soil cover, and facet-to-colluvial-wedge transition?
3. What is the predicted relationship between facet gradient and erosion rate?

We explore these questions with a systematic parameter exploration, beginning with the simple case of a purely weathering-limited slope.

## 5 Results

### 5.1 Weathering Limited Case: Facet Dissolution

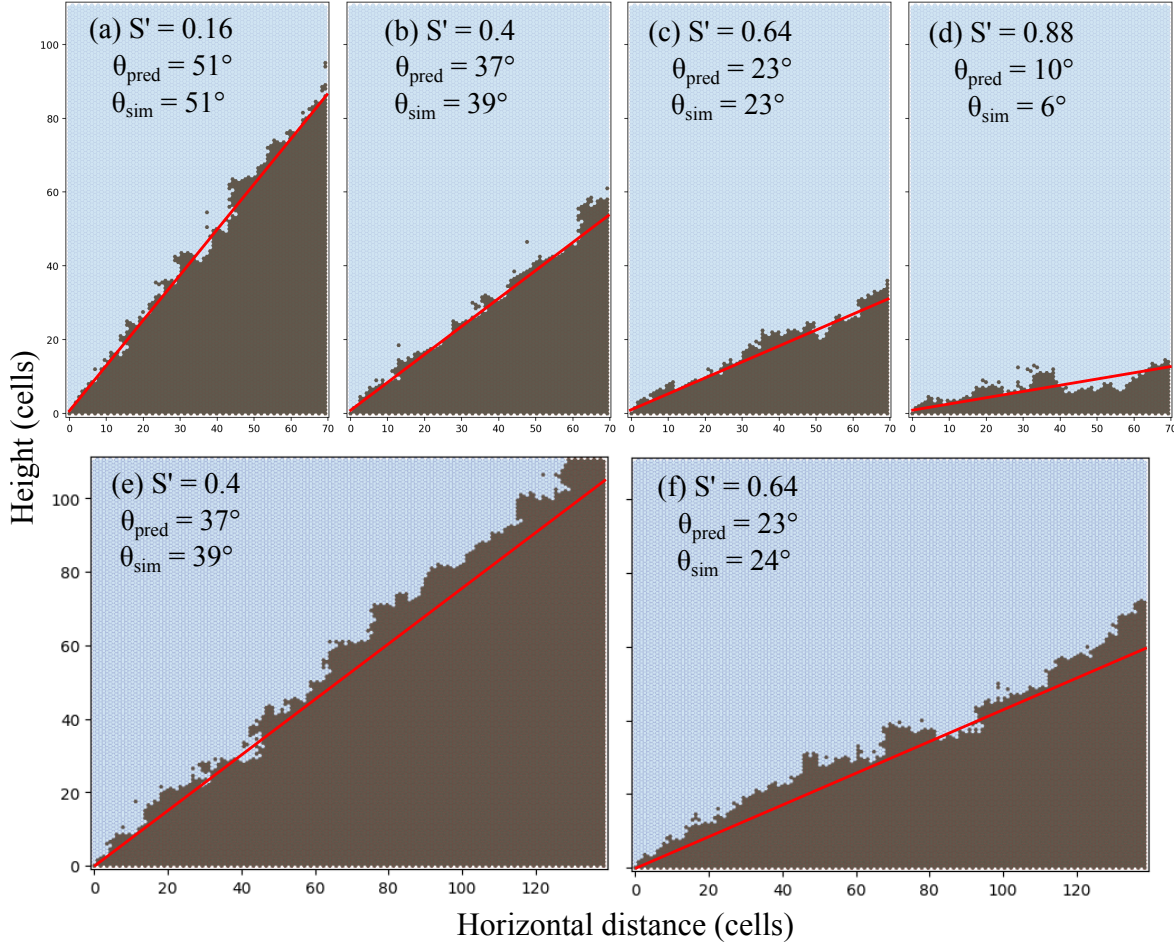
We start with a simple test: if a facet erodes at a steady, uniform rate, its evolution should follow the geometry illustrated in Figure 2. The profile should be linear, and the dip angle should relate to the rates of erosion and slip according to equation (1). To perform this test, we run the model with dissolution activated, and without any rock-to-regolith conversion. The expected average rate of erosion by dissolution is  $E = 2\delta s$ . To simplify the analysis, we define a dimensionless dissolution efficiency as

$$S' = \frac{2\delta s}{V}. \quad (3)$$

The expected facet dip angle is

$$\theta = \alpha - S', \quad (4)$$

where  $\theta$  and  $\alpha$  are both in radians. Figure 5 presents simulated profiles for facets eroded by dissolution, under different values of dimensionless weathering rate  $S'$ . The figure also compares narrow and wide facets. The simulated facets show a linear relation between angle and dissolution rate, consistent with the analytical expectation (equation 1) (Figure 6). As expected, there is no apparent relation between slope angle and the width of the cross section.



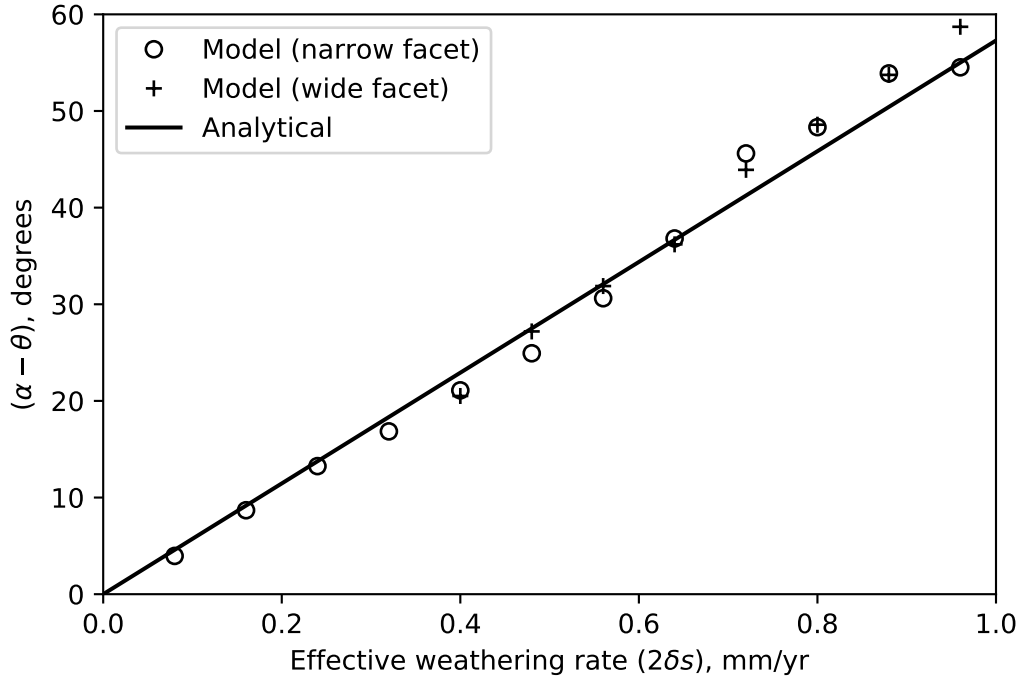
307 **Figure 5.** Simulated facet cross-sectional profiles formed under a combination of fault slip  
 308 and dissolution. Dark gray indicates rock, and light blue is air. Labels show the dimensionless  
 309 effective dissolution efficiency,  $S'$  (equation 3), and the predicted and simulated average facet  
 310 slope angle,  $\theta$ . Line shows facet profile predicted by equation (4).

## 315 5.2 Facets with Regolith

316 We next consider the case in which rock weathers iso-volumetrically to regolith,  
 317 with regolith motion driven by stochastic disturbance events (Figure 4). Two dimension-  
 318 less parameters determine the model's behavior:

$$\text{Dimensionless weathering rate: } w' = w\tau$$

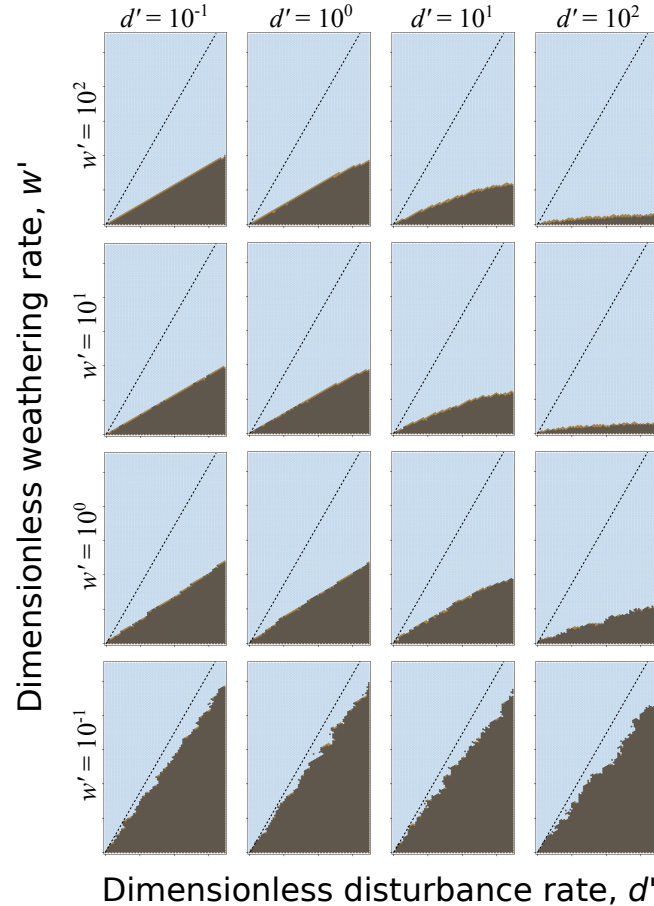
$$\text{Dimensionless disturbance rate: } d' = d\tau.$$



311 **Figure 6.** Difference in angle between fault plane ( $\alpha$ ) and facet ( $\theta$ ), as a function of the  
 312 nominal dissolution rate  $2\delta s$ , from runs with fault slip and dissolution (only). Open circles and  
 313 plusses show individual model runs with a narrow and wide horizontal domain, respectively (see  
 314 Figure 5). Line shows the prediction of equation 5.

319 Figures 7 and 8 illustrate the role of these two parameters for the case of a facet of fixed  
 320 width. The model shows three behavior regimes. When  $w' \gg d'$ , gradient depends on  
 321 the disturbance frequency regardless of weathering rate. In this the transport-limited  
 322 regime, solutions with  $d' \leq 1$  represent angle-of-repose slopes (recall that the model has  
 323 a  $30^\circ$  effective angle of repose). Although these angle-of-repose solutions are not inevitable,  
 324 they occupy a large part of the model's parameter space and could be thought of as a  
 325 sort of attractor state. When  $w' < 1$ , slope angle depends primarily on  $w'$ . But even  
 326 in this weathering-controlled regime, disturbance rate continues to have some influence,  
 327 except in the extreme dissolve-limited case when there is no regolith to move (Figure 8,  
 328 solid curve and circles).

329 Facet length has very little influence on slope angle (compare Figure 8 left and right),  
 330 except in the case of  $d' \gg 1$  (star and triangle symbols in Figure 8). Here, longer slopes  
 331 are systematically steeper.

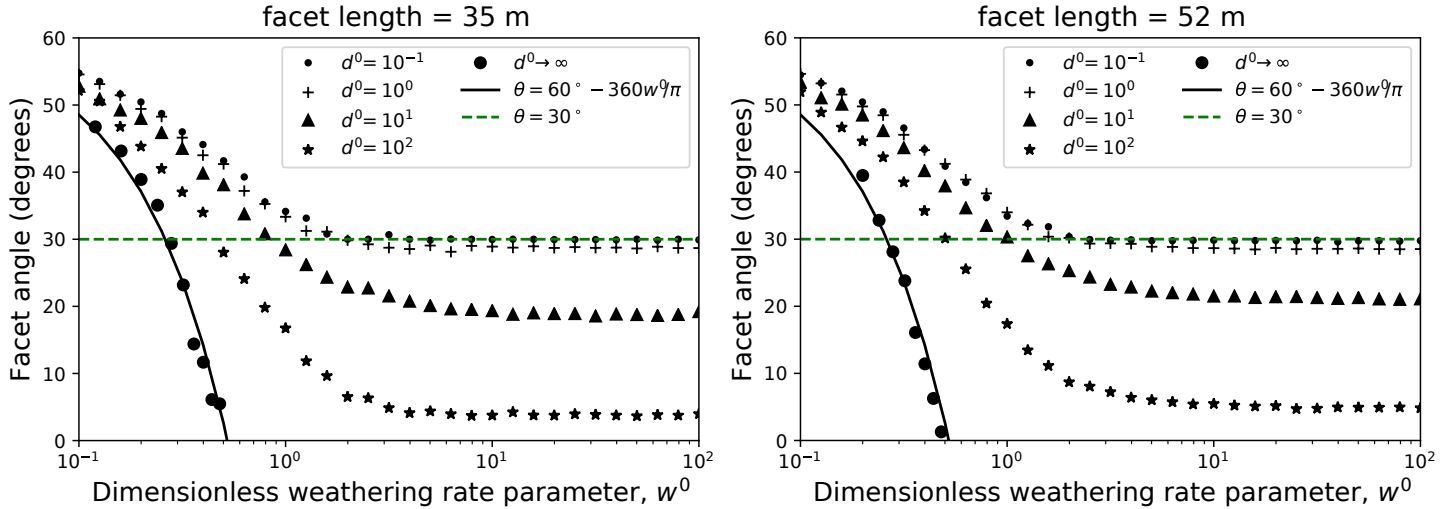


332 **Figure 7.** Examples of simulated facet profiles at varying values of  $d'$  and  $w'$ . Dotted line  
 333 shows projected fault plane.

338 The fractional regolith cover depends mainly on  $w'$  (Figure 9). The re-  
 339 lation follows a sigmoid-like curve, with nearly 90% or greater cover when  $w' > 20$ , and  
 340 less than 50% cover when  $w' < 1$ . For a given  $w'$ , a facet with a higher disturbance rate  
 341 will tend have a thinner cover, all else equal.

### 344 5.3 Colluvial Wedges

345 We explore the formation of colluvial wedges with a series of model runs similar  
 346 to those in Figure 7 but with the fault location shifted to the right (Figure 10). This ge-



334 **Figure 8.** Modeled equilibrium facet angle as a function of weathering and disturbance rate  
 335 parameters. Solid line shows the analytical solution for the case in which no regolith is produced  
 336 (all rock dissolves), which corresponds to an effectively infinite disturbance rate. Dashed line  
 337 shows the model's 30° effective angle of repose.

347 ometry places the baselevel outboard of the fault trace, thereby allowing the creation of  
 348 a colluvial wedge between the fault and baselevel. In the angle-of-repose regime, with  
 349  $w' > 1$  and  $d' \leq 1$ , the wedge shares the same slope gradient as the facet itself, so that  
 350 the fault trace appears partway up the facet slope (Figure 10, upper left). Solutions with  
 351 a lower  $w'$  ...

354 ...then introduce question of colluvial wedges

355 ...then step back and consider whether we've covered it all up to here

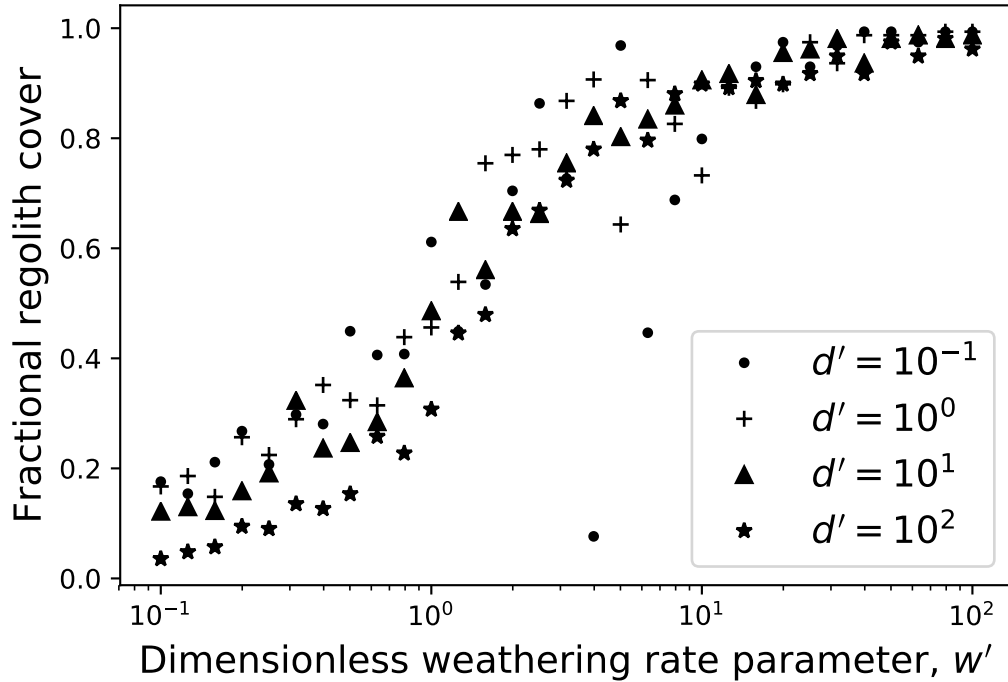
## 356 NOTES

357 pausing here to ponder this... what's needed to give angrep? In a diss-lim world  
 358 it's irrelevant but consider anyway what s' you need to get more than angrep:

$$\theta_c = \alpha - s'_c$$

$$s'_c = \alpha - \theta = 30^\circ \approx 0.52$$

359 So in principle this would apply to  $w'$  too: any less than about 0.5 and it's too steep to  
 360 be ang rep. Lower  $d'$  just makes it worse because the slope is partly covered and weath-  
 361 ering rate goes down.



342 **Figure 9.** Modeled regolith cover proportion for steady facets, as a function of weathering and  
 343 disturbance rate parameters. Scatter around the sigmoidal curve reflects stochastic variability.

362 but the above is consistent with the plot at least: solutions with  $w' < 0.5$  are never  
 363 tlim/ang rep. The actual cutoff seems to be closer to 1 or 2 as a minimum  $w'$ . But you  
 364 also apparently need  $d' \leq 1$ . Why? Presumably if you have lots of soil but disturb it  
 365 faster than tectonics pushes it up, erosion “wins” and keeps at least parts of the slope  
 366 below angrep.

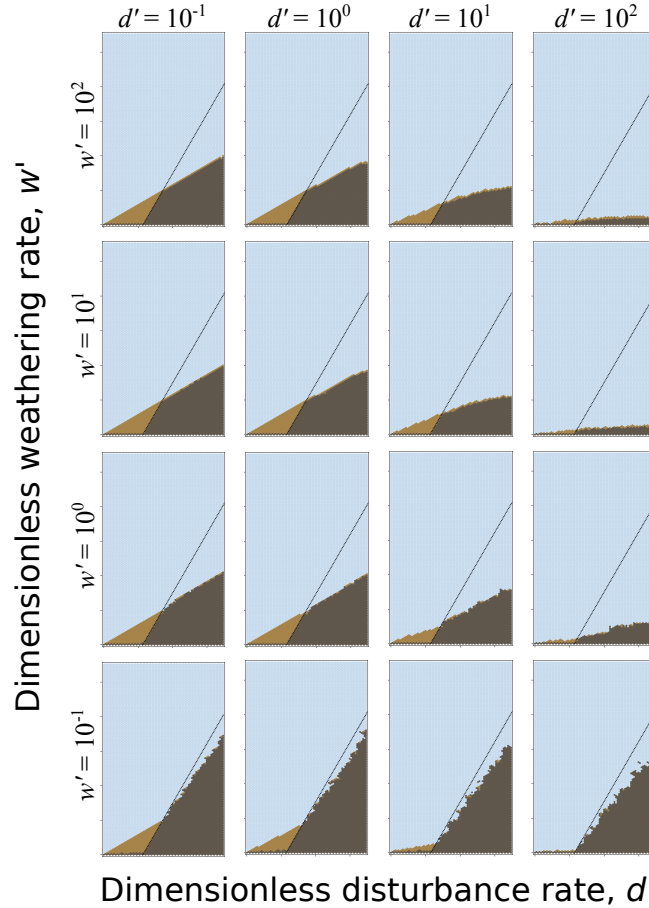
367 note that being on average below angrep doesn’t mean lower part isn’t angrep. de-  
 368 pends on length.

#### 369 IV. Results

##### 370 A. Weathering-limited facets

371 demonstrate that one recaptures Tucker et al. 2011 behavior when  $d' \ll w'$ : ex-  
 372 periments in which the predicted angle should be 60 degrees (no weathering), 45, 30, 15.

##### 373 B. Influence of $d'$ and $w'$



352 **Figure 10.** Simulated facet profiles showing the development of a colluvial wedge on the  
353 hangingwall.

374 3x3 (or maybe 5x5) plot in  $d'$  and  $w'$  space

375 plot of facet dip angle in  $d'$  and  $w'$  space (from talk, showing family of curves)

376 C. (optional) what if rock or soil can dissolve, a la Italian carbonates? (dissolution  
377 rule)

378 D. (optional) baselevel effects - what happens when either you have a basal stream  
379 cutting down or a hangingwall valley aggrading? This would require having a modifi-  
380 cation that would add or remove rock cells along the left edge

381 E. what sets the effective E vs S relation? refer back to T et al., 2011, noting re-  
382 strictive assumption of slope-independent erosion rate

383 F. (optional) how could one mimic the effective rule in a differential equation world?

384 Try out something like the depth-dependent Taylor model.

385 **V. Discussion**

386 - model accounts for basic morphology and shape. necessary and sufficient condi-  
 387 tions for planar facet with dip angle less than fault dip: weathering of rock plus distur-  
 388 bance, and [something about limits, i.e., curvature appears when  $d'/w' > \dots$ ]

389 - facet angle close to angle of repose is an attractor state, because below that an-  
 390 gle, the transport rate and length scale of produced regolith goes way down

391 - for this reason, it should be common to observe cases where the fault trace cuts  
 392 across a roughly uniform slope, marking a transition from eroding rock to aggrading col-  
 393 luvium

394 - cases that do NOT show this morphology are anomalies, likely reflecting strong  
 395 baselevel control apart from simply fault slip (aggradation or incision)

396 - facet dip angle is set by ...

397 - facet soil cover depth and spatial continuity set by ...

398 - facets are predicted to become concave-up when ...

399 - to test these ideas, we need cosmos on facet slopes!

400 **VI. Conclusions**

401 model accounts for facet morphology as a consequence of tectonic motion, rock weath-  
 402 ering and regolith disturbance

403 variations in facet morphology can be explained as a consequence of ...

404 erosion rate does depend on slope gradient, like thus-and-such

405 need cosmos to test these predictions

406 **TENTATIVE LIST OF FIGURES:**

407 - pix of facets

408 o bar graph of regolith thickness and percent cover on a bunch of facets

- 409 - model illustration combining list of states with hexagons, with schematic exam-  
 410 ple transitions from Grain Hill
- 411 - T et al 2011 schematic
- 412 = figure showing model diss-lim runs at varying S', compared with analytical
- 413 - model vs analytical diss-lim
- 414 - 4x4 of sim profiles in d' vs w' space
- 415 - plot of gradient in d' and w' space
- 416 - same for reg cover proportion
- 417 (o illustration with baselevel lowering)
- 418 - illustration with baselevel rise
- 419 o illustration with time-varying w and/or d

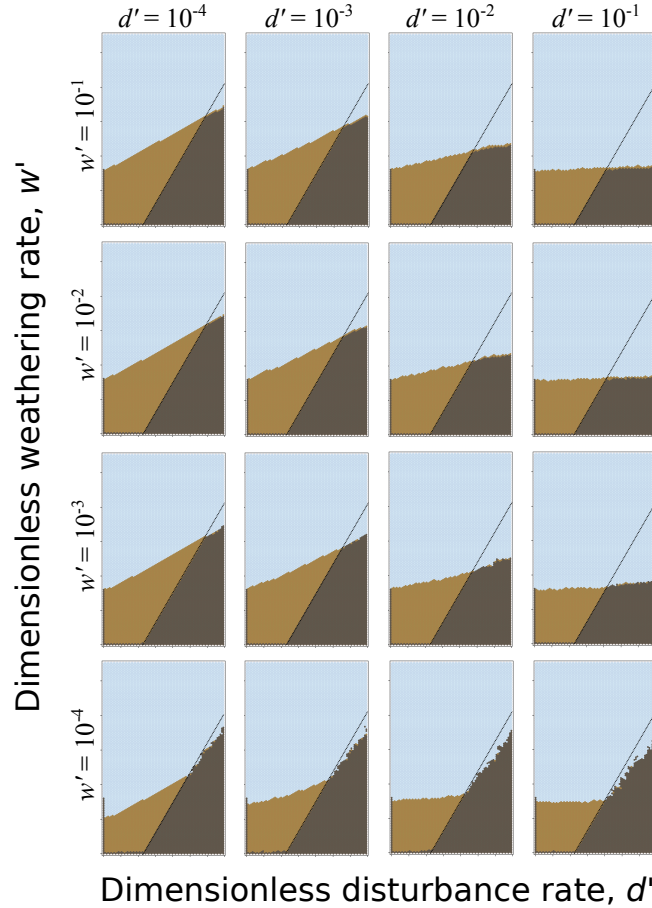
$$\alpha - \theta = E/V \quad (5)$$

## 422 Acknowledgments

423 NSF normal faults, landlab, csdms, ...

## 424 References

- 425 Anderson, T. C. (1977), Compound faceted spurs and recurrent movement in the  
 426 Wasatch Fault zone, north central Utah, Ph.D. thesis, Brigham Young University.
- 427 Blackwelder, E. (1928), The recognition of fault scarps, *The Journal of Geology*,  
 428 36(4), 289–311.
- 429 Boulton, S., and A. Whittaker (2009), Quantifying the slip rates, spatial distribution  
 430 and evolution of active normal faults from geomorphic analysis: Field examples  
 431 from an oblique-extensional graben, southern turkey, *Geomorphology*, 104 (3-4),  
 432 299–316.
- 433 Bras, R., G. Tucker, and V. Teles (2003), Six myths about mathematical model-  
 434 ing in geomorphology, in *Prediction in Geomorphology*, edited by P. Wilcock and  
 435 R. Iverson, pp. 63–79, American Geophysical Union.



420      **Figure 11.** Simulated facet profiles with a rising baselevel along the left model boundary,  
 421      representing an aggrading hangingwall basin.

- 436      Bubeck, A., M. Wilkinson, G. P. Roberts, P. Cowie, K. McCaffrey, R. Phillips, and  
 437      P. Sammonds (2015), The tectonic geomorphology of bedrock scarps on active  
 438      normal faults in the Italian Apennines mapped using combined ground penetrating  
 439      radar and terrestrial laser scanning, *Geomorphology*, 237, 38–51.
- 440      Davis, W. M. (1903), The mountain ranges of the great basin, *Harvard University*  
 441      *Museum of Comparative Zoology Bulletin*, 40(3), 129–177.
- 442      Davis, W. M. (1909), *Geographical Essays*, Ginn.
- 443      Densmore, A. L., M. A. Ellis, and R. S. Anderson (1998), Landsliding and the evo-  
 444      lution of normal-fault-bounded mountains, *Journal of Geophysical Research*, 103,  
 445      15,203–15,219.
- 446      DePolo, C., and J. Anderson (2000), Estimating the slip rates of normal faults in the  
 447      great basin, USA, *Basin Research*, 12(3–4), 227–240.

- 448 Ellis, M., A. Densmore, and R. Anderson (1999), Development of mountainous to-  
449 topography in the basin ranges, usa, *Basin Research*, 11(1), 21–42.
- 450 Fuller, R. E. (1931), The geomorphology and volcanic sequence of Steens Mountain  
451 in southeastern Oregon, *University of Washington Publications in Geology*, 3(1).
- 452 Furbish, D., P. Haff, W. Dietrich, and A. Heimsath (2009), Statistical description of  
453 slope-dependent soil transport and the diffusion-like coefficient, *J. Geophys. Res.*,  
454 114, F00A05.
- 455 Gilbert, G. (1928), *Studies of basin-range structure*, U. S. Geological Survey Profes-  
456 sional Paper, vol. 153, United States Government Printing Office.
- 457 Gilluly, J. (1928), Basin range faulting along the Oquirrh Range, Utah, *Bulletin of*  
458 *the Geological Society of America*, 39(4), 1103–1130.
- 459 Hamblin, W. (1976), Patterns of displacement along the wasatch fault, *Geology*,  
460 4(10), 619.
- 461 Menges, C. (1990), Soils and geomorphic evolution of bedrock facets on a tectoni-  
462 cally active mountain front, western Sangre de Cristo Mountains, New Mexico,  
463 *Geomorphology*, 3(3-4), 301–332.
- 464 Pack, F. J. (1926), New discoveries relating to the Wasatch fault, *American Journal*  
465 *of Science*, 11(65), 399–410.
- 466 Petit, C., Y. Gunnell, N. Gonga-Saholiariliva, B. Meyer, and J. Seguinot (2009),  
467 Faceted spurs at normal fault scarps: Insights from numerical modeling, *Journal*  
468 *of Geophysical Research—Solid Earth*, 114, doi:10.1029/2008JB005955.
- 469 Schneider, H. (1925), A discussion of certain geologic features of the Wasatch Moun-  
470 tains, *The Journal of Geology*, 33(1), 28–48.
- 471 Strak, V., S. Dominguez, C. Petit, B. Meyer, and N. Loget (2011), Interaction be-  
472 tween normal fault slip and erosion on relief evolution: Insights from experimental  
473 modelling, *Tectonophysics*, 513(1-4), 1–19.
- 474 Struble, W. T., S. W. McCoy, D. E. J. Hobley, G. E. Tucker, and L. C. Gregory (in  
475 review), Mountain-Front Facet Gradient Encodes Long-Term Slip Rate Along the  
476 Wasatch Normal Fault, USA, *TBD*.
- 477 Tucker, G., S. McCoy, A. Whittaker, G. Roberts, S. Lancaster, and R. Phillips  
478 (2011), Geomorphic significance of postglacial bedrock scarps on normal-fault  
479 footwalls, *Journal of Geophysical Research*, 116(F1), F01,022.

- 480 Tucker, G. E., D. E. Hobley, E. Hutton, N. M. Gasparini, E. Istanbulluoglu, J. M.  
481 Adams, and S. S. Nudurupati (2016), Celllab-cts 2015: continuous-time stochas-  
482 tic cellular automaton modeling using landlab, *Geoscientific Model Development*,  
483 9(2), 823–839.
- 484 Tucker, G. E., S. W. McCoy, and D. E. Hobley (2018), A lattice grain model of  
485 hillslope evolution, *Earth Surface Dynamics*, 6(3), 563–582.
- 486 Wallace, R. (1978), Geometry and rates of change of fault-generated range fronts,  
487 north-central Nevada, *Journal of Research of the U.S. Geological Survey*, 6(5),  
488 637–650.
- 489 Wilkinson, M., G. P. Roberts, K. McCaffrey, P. A. Cowie, J. P. F. Walker, I. Pa-  
490 panikolaou, R. J. Phillips, A. M. Michetti, E. Vittori, L. Gregory, et al. (2015),  
491 Slip distributions on active normal faults measured from LiDAR and field map-  
492 ping of geomorphic offsets: an example from L’Aquila, Italy, and implications for  
493 modelling seismic moment release, *Geomorphology*, 237, 130–141.
- 494 Zuchiewicz, W. A., and J. P. McCalpin (2000), Geometry of faceted spurs on an  
495 active normal fault: case study of the central wasatch fault, utah, usa, in *Annales  
496 Societatis Geologorum Poloniae*, vol. 70, pp. 231–249.